Solar Energy 183 (2019) 812–822

Contents lists available at ScienceDirect

Solar Energy

journal homepage: www.elsevier.com/locate/solener

Simulating the energy yield of a bifacial photovoltaic power plant

Dimitrij Chudinzow[a,*], Jannik Haas[b], Gustavo Díaz-Ferrán[c], Simón Moreno-Leiva[a], Ludger Eltrop[a]

[a] Institute of Energy Economics and Rational Energy Use (IER), University of Stuttgart, Heßbrühlstraße 49a, 70565 Stuttgart, Germany
[b] Department of Stochastic Simulation and Safety Research for Hydrosystems (IWS/SC SimTech), University of Stuttgart, Pfaffenwaldring 5a, 70569 Stuttgart, Germany
[c] Energy Center, Department of Electrical Engineering, University of Chile, Tupper 2007, Santiago, Chile

ARTICLE INFO

Keywords:
PV
Optical model
Ground-reflected irradiance
Albedo
Chile

ABSTRACT

Bifacial photovoltaics (bifacial PV) offer higher energy yields as compared to monofacial PV. The development of appropriate models for simulating the energy yield of bifacial PV power plants is a major topic in both research and industry. In particular, the adequate calculation of the energy yield from ground-reflected irradiance (GRI) is challenging. The purpose of this work is to investigate the currently available energy yield models and suggest areas for improvement. A new model with the proposed enhancements is used to investigate the behaviour of bifacial PV power plants in more detail. The model calculates the absorbed irradiation originating from eight irradiance contributions for the front and rear of each cell string: DNI, DHI, GRI from DHI (GRI_{DHI}) and GRI from DNI (GRI_{DNI}). The model was tested using a defined case study power plant. The breakdown of absorbed irradiation (subscript "ab") into its contributions revealed that while in summer months $GRI_{DNI\text{-}ab\text{-}rear}$ is significantly larger than $GRI_{DHI\text{-}ab\text{-}rear}$, both are roughly the same in winter months. Furthermore, for the calculation of GRI the common simplification of infinitely long module rows was avoided by implementing an algorithm for the view factor calculation for a three-dimensional space. This procedure allowed for the assessment of impact of the ground size on the annual energy yield. In a sensitivity analysis, it has been shown that the extension of the relevant ground area resulted in an asymptotical increase of the energy yield. Additionally, the impact of ground shadows on the power plant's performance was quantified. The presence of ground shadows reduced the annual electricity generation by almost 4%, compared to a hypothetical scenario where no ground shadows existed. Finally, five different ground surfaces and the resulting bifacial gains were analysed. The results show that while dry asphalt (12% reflectivity) gave less than 6% of bifacial gain related to generated electricity (BG_{el}), the use of a white membrane (70%) would result in 29% of BG_{el}.

1. Introduction

Although bifacial PV is known since the 1950s, it was considered as a niche technology for decades (Kopecek, 2014). The main advantage of this technology is its ability to utilize irradiation on the back of a PV cell, thereby increasing the energy yield per unit of land use. For example, the experimental 1.25 MW fixed-tilt bifacial Hokuto PV power plant in Japan showed a bifacial gain related to generated electricity (BG_{el}) of almost 20% over the course of more than two years (Ishikawa, 2016). Nevertheless, the interest in bifacial PV is growing. The worldwide installed bifacial PV capacity was at 1 GW by the end of 2017 (Kopecek and Libal, 2018). The "International Technology Roadmap for Photovoltaic" predicted that 30% of annually sold c-Si PV modules will be bifacial by the year 2030 (VDMA, 2017).

A significant barrier for the further propagation of bifacial PV systems is the lack of established methods to predict the energy yield of bifacial PV systems (Meydbray, 2018). Reliable yield predictions are mandatory for a bank to finance a new power plant. Yield predictions, which are associated with a higher uncertainty, lead to a higher risk premium and consequently to higher project costs (Richter, 2017). Ultimately, this issue has been stalling a more extensive use of bifacial PV technology. To overcome this, a fundamental understanding of the behaviour of bifacial PV systems is essential to support the development of more reliable yield models. Below, we give a brief overview of the related studies, highlight the main assumptions and explore the potential for improvements.

The annual energy yield of ground-mounted fixed-tilt bifacial PV arrays and one-axis tracked stand-alone bifacial modules was simulated by Shoukry et al. (2016). To calculate the bifacial gain related to generated electricity (BG_{el}), the ground area was divided into two segments: shaded and unshaded. The shaded ground segment reflected diffuse irradiance only, whereas the unshaded ground reflected both

* Corresponding author.
E-mail address: dimitrij.chudinzow@ier.uni-stuttgart.de (D. Chudinzow).

https://doi.org/10.1016/j.solener.2019.03.071
Received 22 June 2018; Received in revised form 18 March 2019; Accepted 19 March 2019
Available online 27 March 2019
0038-092X/

Nomenclature

Abbreviation and explanation

$DNI_{ab\text{-}front/rear}$, $DHI_{ab\text{-}front/rear}$, $GRI_{DNI\text{-}ab\text{-}front/rear}$, $GRI_{DHI\text{-}ab\text{-}front/rear}$ *Absorbed irradiation:* Absorbed irradiation (subscript "ab") from corresponding irradiance contribution (Wh)

T_{amb} *Ambient air temperature:* Temperature of ambient air. Taken from "Typical Meteorological Year" (TMY) dataset (°C)

θ, θ_Z *Angle of incidence of beam irradiance:* Angle of incidence θ on an inclined surface (module) and on a horizontal surface (ground) θ_Z (DEG)

$A_{String,\ unshaded}$, $A_{String,\ shaded}$ *Area of an unshaded or shaded cell string:* $A_{String,\ unshaded} = \frac{\text{Module area}}{\text{Number of cell strings per module}}$. If a cell string is partly shaded, $A_{string,\ shaded}$ is the remaining unshaded area of the cell string. If a cell string is fully shaded, $A_{string,\ shaded}$ is zero (m^2)

$A_{FVF/RFV_{complete/reduced}}$ *Area of complete/reduced front view field/rear view field:* A "complete" view field describes the rectangular view field of a module row, whose edges do not overlap with a ground shadow. When the edges of a view field overlap with ground shadow(s), the shape of the original view field minus the part(s) of ground shadow(s) that overlap(s) with the view field defines a "reduced" view field (m^2)

BG_{ab} *Bifacial gain related to absorbed irradiation:* $\frac{\text{Absorbed irradiation by rear of bifacial PV system}}{\text{Absorbed irradiation by front of bifacial PV system}}$ (–)

BG_{el} *Bifacial gain related to generated electricity:* $\frac{\text{Generated electricity by rear of bifacial PV system}}{\text{Generated electricity by front of bifacial PV system}}$ (–)

ϕ_{PV} *Bifaciality:* Ratio of rear and front electrical efficiency; $\phi_{PV} = \frac{\eta_{PV,\,el,\,rear}}{\eta_{PV,\,el,\,front}}$. In this work $\phi_{PV} = 0.85$ (–)

T_0 *Critical temperature:* Temperature at which η_{PV} is zero. Set to 270 °C (Dubey et al., 2013) (°C)

DHI *Diffuse horizontal irradiance:* Direct horizontal irradiance; this irradiance contribution is considered isotropic (Duffie and Beckman, 2013) ($\frac{W}{m^2}$)

DNI *Direct normal irradiance:* Direct normal irradiance ($\frac{W}{m^2}$)

$\eta_{PV,\,front/rear}$ *Electrical efficiency:* Electrical efficiency of PV module (–)

GE *Generated electricity:* Generated electricity by the bifacial PV power plant (Wh)

GR *Ground reflectivity:* $\frac{\text{Reflected irradiance by the ground}}{\text{Received irradiance by the ground}}$, $[0 \le GR \le 1]$ (–)

GRI_{DHI} *Ground-reflected DHI:* Diffuse horizontal irradiance, which is reflected by the ground. This irradiance contribution is considered isotropic ($\frac{W}{m^2}$)

GRI_{DNI} *Ground-reflected DNI:* Direct normal irradiance, which is reflected by the ground. This irradiance contribution is diffuse and considered isotropic ($\frac{W}{m^2}$)

I_{NOCT} *Irradiance at NOCT:* Irradiance at which NOCT is measured ($I_{NOCT} = 800\ W/m^2$) ($\frac{W}{m^2}$)

α_{PV} *Irradiation absorption factor of PV module:* $\frac{\text{Absorbed irradiation by PV module}}{\text{Received irradiation by PV module}}$, $[0 \le \alpha_{PV} \le 1]$. In this work = 0.95 (–)

NOCT *Nominal operating cell temperature:* PV cell temperature at I_{NOCT} and 25 °C ambient air temperature. In this work $T_{NOCT} = 43$ °C

T_{ref} *Reference temperature:* Temperature at which $\eta_{PV,\,el,\,ref}$ is given. In this work $T_{ref} = 25$ °C

SEY *Specific electricity yield:* Generated electricity per installed front-side capacity ($\frac{Wh_{dc}}{W_{front}}$)

β *Temperature coefficient of* η_{PV}: $\frac{1}{T_0 - T_{ref}}$ ($\frac{1}{°C}$)

$E_{ab_{String,\,front/rear}}$, $E_{el_{String}}$ *Total absorbed irradiation and generated electricity by cell string:* Total absorbed irradiation and generated electricity by a cell string. If a string is partially or fully shaded, the generated electricity is zero due to activated bypass diode (Wh, Wh_{dc})

I_{sum} *Total irradiance:* Sum of all irradiance contributions ($\frac{W}{m^2}$)

$V_{Cell\ String \rightarrow Sky}$ *View factor from cell string to sky:* View factor of a cell string to the sky. For front side of first row and rear side of last row calculated according to (Yusufoglu et al., 2014). View factors for front sides of second till last row and rear sides of first till penultimate row calculated following (Maor and Appelbaum, 2012), $[0 \le V_i \le 1]$ (–)

$V_{FVF/RVF_{complete/reduced} \rightarrow Cell\ String}$ *View factor from view field to cell string:* View factor of a complete or reduced view field to a cell string. $0 \le V_{FVF/RVF_{complete/reduced} \rightarrow Cell\,string} \le 1$. View factors calculated numerically using (Lauzier, 2004) (–)

VF width factor *View fields' width factor:* Describes by which factor the width of a view field is enlarged to the left and to the right hand side of a module row. A value of zero means, that the width of a view field equals the length of a module row. Setting the value, for example, to 0.5 would mean that the width is enlarged by 50% of a module row's length to the left and to the right hand side. The resulting total width of the view field would be 200% of a module row's length (–)

beam and diffuse irradiance. The ratio of ground-reflected irradiance (GRI) that reached a cell on the back was calculated using the concept of view factors (Stephan et al., 2010), assuming that ground shadows are always rectangular (Gross et al., 1981). Considering the shape of ground shadows to be mostly oblique parallelograms is one option to increase the precision of energy yield models. Furthermore, the authors assumed that the GRI of a row is influenced by the two adjacent rows only. Since the investigated PV array had three rows, the middle row was influenced by the two other rows, while the other two were influenced by the middle row only. As we will show in Section 2.3, it can happen that a module row's energy yield is affected by more than two rows. This understanding provides further possibility for the improvement of energy yield models. Finally, GRI was neglected for the front, thus underestimating the total energy yield.

A simulation tool for the power generation of a fixed-tilt bifacial PV power plant was developed by Chiodetti et al. (2015). The investigated power plant had three rows, each with 14 modules. The power generation of the back row was calculated by differentiating between shaded and unshaded ground areas and applying the corresponding view factors. In order to reduce computation time, view factors were calculated for one day per month and interpolated. The relative error on annual energy yield was calculated for different slopes and locations and showed that the maximum error was below 0.2%. Nevertheless, with other module slopes or at other locations, the error might be higher. Avoiding interpolation of view factors can eliminate a source of uncertainty.

The annual absorbed irradiation and bifacial gain related to absorbed irradiation (BG_{ab}) of vertically mounted and optimally inclined bifacial arrays were investigated by Appelbaum (2016). Since the ground was not subdivided into shaded and unshaded areas, the obtained results very likely overestimated the energy yield. Therefore, the distinction of shaded and unshaded ground for calculating GRI is considered as a necessity for all energy yield models.

An approach to simulate the energy yield per unit of used land of vertically mounted bifacial PV arrays was presented by Khan et al. (2017). The annual energy yield of optimally tilted (tilt angle of module rows correspond to the latitude) monofacial and vertically mounted bifacial PV arrays was compared for several locations worldwide,

particularly taking into account the latitude and local irradiance conditions. While the GRI was considered for bifacial PV arrays, it was neglected for the monofacial ones, thus making the comparison somewhat unbalanced. The calculation of view factors related to GRI was based on the assumption of infinitely long module rows. While this is a common assumption since it allows for the analytical (and therefore quick) calculation of view factors, one cannot investigate some important parameters (e.g., effect of increasing the ground area, which contributes to GRI).

NREL's System Advisor Model (SAM) is a well-known tool to model and evaluate renewable energy technologies. Currently, SAM's technology portfolio is being enhanced with bifacial PV power plants (DiOrio and Deline, 2018). Keeping the computation time of view factors low was crucial to the developers; therefore, the assumption of infinitely long module rows was applied. The calculation of GRI is performed by meshing the space between two rows into *n* segments, labelling each segment as either shaded or unshaded, and finally applying view factors both to shaded and unshaded segments (Marion et al., 2017). It is a principal question, whether a model shall be particularly fast or precise. As the understanding of bifacial PV systems' behaviour grows, the decision about which parameter needs to be modelled in more or less detail will be made simpler.

PVsyst is probably the most popular commercial simulation software for PV systems. In 2017, PVsyst's approach to implement bifacial PV systems was presented in Mermoud and Wittmer (2017). For the fast computation of GRI, PVsyst also makes use of the two-dimensional view factor calculation. Using masking angles, the amount of irradiance hitting the ground from sky is calculated in a two-dimensional manner. It remains unclear which time resolution was used for the view factor calculation and whether or not the user can edit it. Based on a sensitivity analysis, the authors recommend slightly higher tilt angles for bifacial than for monofacial PV systems for achieving maximum energy yield.

MoBiDiG is another tool to predict the energy yield of bifacial systems and to calculate the levelized cost of electricity (Berrian et al., 2017). It calculates the absorbed irradiation according to the aforementioned work from Shoukry et al. (2016) as well as the current and voltage at the maximum power point for each module. The model was validated against a test system installed on a building roof. The reported mismatch of modelled and measured power from five aggregated days was 4.9%.

A three-dimensional calculation of view factors for calculating GRI was implemented in the tool BIGEYE (Janssen et al., 2018). BIGEYE accounts for self-shading, shading from nearby objects and homogeneous transparency of the modules. Additionally, energy yield simulations for one-axis tracked systems are possible. Using an experimental rooftop installation in Zurich, the model was validated against generated electricity for a sunny day for different tilt angles. The relative deviations were below 4%, although it should be noted that using data from a single day only might be insufficient.

In summary, for an adequate simulation of bifacial PV power plants the distinction of shaded and unshaded ground segments is mandatory. To account for GRI, the theory of view factors seems to be the method of choice. Although the assumption of infinitely long module rows is convenient, since it allows using analytical functions for the quick calculation of view factors, a three-dimensional calculation of view factors might provide deeper insights into the behaviour of bifacial PV systems.

This work aims to provide a deeper understanding about the behaviour of bifacial PV power plants by including the following considerations:

1. The calculation of absorbed irradiation for both sides of each cell string originating from eight irradiance contributions: DNI_{front}, DNI_{rear}, DHI_{front}, DHI_{rear}, $GRI_{DNI\text{-}front}$, $GRI_{DNI\text{-}rear}$, $GRI_{DHI\text{-}front}$, $GRI_{DHI\text{-}rear}$, as well as generated electricity (direct current). The breakdown of the absorbed irradiation into its components indicates the importance of each contribution to the energy yield.
2. Avoiding the assumption of infinitely long module rows for calculating GRI. Instead, the view factor between the relevant ground area and a cell string was computed with a numerical algorithm in three-dimensional space. This allowed for quantification of the impact of the ground size on the energy yield.
3. The quantification of the impact of cast ground shadows on the power plant's performance.
4. Comparing five ground surfaces (and the corresponding reflectivity), the potential of increasing the energy yield through ground treatment is shown.

In order to make this work more transparent, all analyses were performed for a defined case study of a bifacial PV power plant, which is based on the characteristics of the Chilean bifacial PV power plant La Hormiga (Joanny et al., 2017). The following Section 2 presents the methodological approach. Results are discussed in Section 3. Finally, Section 4 contains a conclusion and an outlook for further research.

2. Method

The basic structure of the model can be subdivided in three parts (Model Inputs, Model Calculations and Results) and is shown in Fig. 1. The model was written in Matlab.

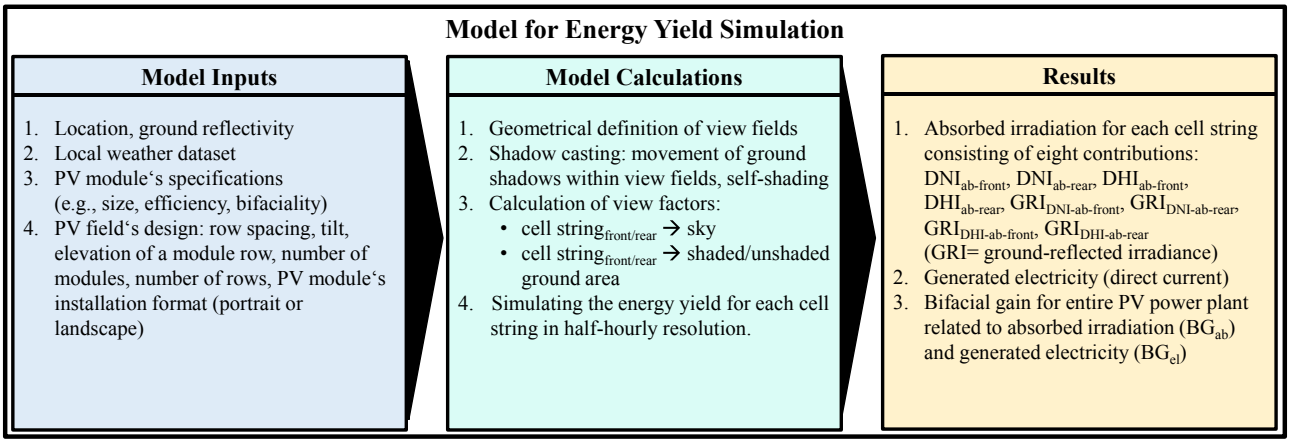

Fig. 1. Structure of the model.

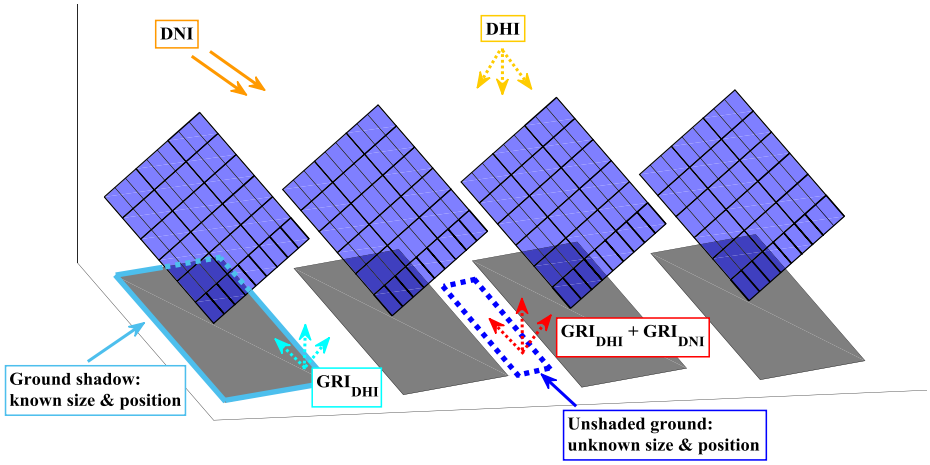

Fig. 2. Irradiance contributions in a bifacial PV array: DNI, DHI, GRI_{DHI} and GRI_{DNI}.

2.1. Irradiance contributions

First, we are going to examine the most relevant irradiance contributions for power generation of bifacial PV systems. In this work, we assumed that the modules were completely opaque; therefore, their cast ground shadows did not receive any beam irradiance (DNI). The isotropic sky diffuse model was used, which means that diffuse irradiance is uniform for the sky dome (Duffie and Beckman, 2013). Fig. 2 shows that only diffuse horizontal irradiance (DHI) is reflected from shaded parts of the ground, thereby producing GRI_{DHI}. In contrast, the unshaded parts of the ground reflect both direct and diffuse irradiance, yielding GRI_{DHI} and GRI_{DNI}. While the position and size of cast ground shadows are relatively easy to simulate, the size and position of the unshaded ground parts is unknown and therefore need to be dealt with differently. To calculate the ground shadows, the spatial position of the modules' corners and the sun's celestial path are the only inputs needed. The simulation of the sun's movement was performed according to Duffie and Beckman (2013). In our model, any configuration of module rows is possible, as long as all module rows are symmetric. The next Section 2.2 describes how the unshaded ground area was accounted for.

2.2. Definition of view fields

To consider for both GRI_{DHI} and GRI_{DNI}, a rectangular ground segment for each side of a module row was defined. We expressed these ground segments as "front view field" and "rear view field". One of our central assumptions is that GRI, which is created outside any view field, does not contribute to absorbed irradiation.

Fig. 3 depicts an example of how the front and rear view fields for module row 3 are defined. The length of the front view field is defined with the pink[1] (PL1, PL2) and green (GL1, GL2) lines in such a way that GRI can hit the top edge of module row 3. The resulting cone, which encloses the space of radiative energy exchange between the front view field and third module row, is coloured green. Accordingly, the pink (PL1, PL2) and turquoise (TL1, TL2) coloured lines define the length of third row's rear view field. The resulting cone, which encloses the space of radiative energy exchange between the rear view field and third module row, is coloured turquoise. The front view field of the first row and the rear view field of the last row are considered to be larger, since they are not obstructed from either side by adjacent module rows. In this work, the length of the first front view field and the last rear view field was defined as 150% of the length of inner view fields. Furthermore, the width of all view fields is equal. The width of the view fields' was defined as the 1.5-fold length of a module row by prolongation of the view fields both to the left and to right by 25% of a module row's length. By performing a sensitivity analysis in Section 3.3, the impact of the view field's width on annual energy yield was investigated.

2.3. Definition of shading constellations

There are two distinct shading constellations: without and with self-shading among the module rows. When there is no self-shading, the shadows on the ground are separated (Fig. 4a). One can also see that a cast ground shadow of a row overlaps with multiple view fields (Fig. 4b), thereby reducing the amount of absorbed GRI_{DNI} for the whole array. As mentioned in Section 1, Fig. 4b illustrates that the cast shadow of a specific module row may easily reduce absorbed $GRI_{DNI\text{-}ab\text{-}front/rear}$ by any other module row: the green ground shadow overlaps with all four front view fields. This effect becomes especially prominent with a lower elevation of the sun's angle and narrow row distances. When self-shading occurs, the cast ground shadows of the equidistantly placed module rows merge into one single shadow segment (Fig. 5a). This single shadow overlaps with three rear view fields and one front view field (Fig. 5b). The shadow part, which is shown in yellow in Fig. 5b, does not contribute to absorbed irradiation, since it is not part of any view field. The described interaction among ground shadows and view fields discourages from analysing isolated module rows. Instead, the PV field should be considered in a holistic manner. The presented model accounts for interactions among any ground shadow, any module row and any view field.

2.4. Calculation of absorbed irradiation

The definition of view fields and the distinction of shaded and unshaded areas of each view field allow the application of the concept of view factors for calculating $GRI_{DNI\text{-}ab\text{-}front/rear}$ and $GRI_{DHI\text{-}ab\text{-}front/rear}$. Both irradiation contributions were calculated for each cell string for both sides, and the corresponding view factors were computed using the numeric algorithm from (Lauzier, 2004), which allows the calculation of view factors for arbitrarily shaped planar surfaces in three-dimensional space. The amount of $DHI_{ab\text{-}front/rear}$ was calculated for each module row as a whole, whereby the corresponding view factors were determined analytically according to Maor and Appelbaum (2012). Finally, the amount of $DNI_{ab\text{-}front/rear}$ was calculated according to Duffie and Beckman (2013). To avoid additional complexity, it was assumed that the view factor from a view field to the sky is always one,

[1] For interpretation of color in Fig. 3, Fig. 4b, Fig. 5a and Fig. 5b, the reader is referred to the web version of this article.

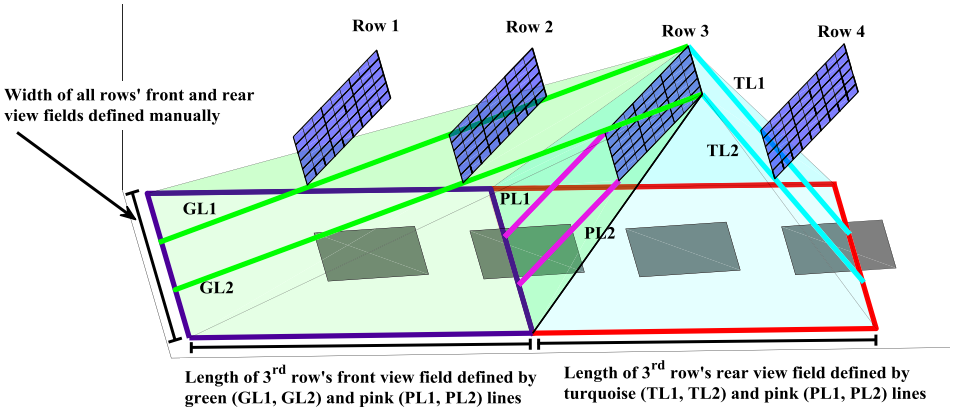

Fig. 3. Example definition of the view fields of module row 3.

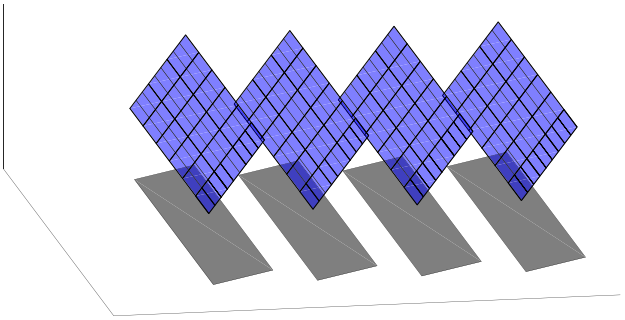

Fig. 4a. Array without self-shading. A single ground shadow is (mostly) shaped as an oblique parallelogram. All ground shadows are separated.

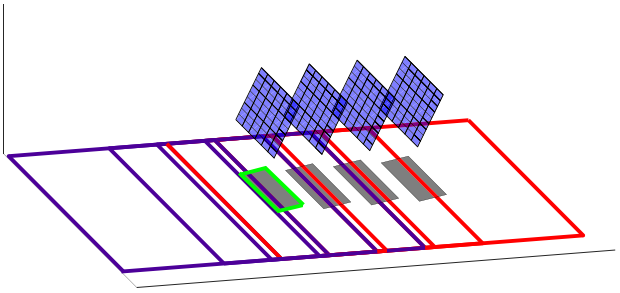

Fig. 4b. Interaction of cast ground shadows with front (purple) and rear (red) view fields at time with no self-shading. The green-contoured shadow overlaps with all four front view fields.

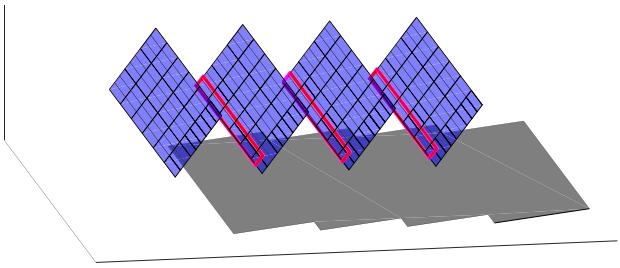

Fig. 5a. Array with self-shading. Cast ground shadows merged into a single shadow polygon. The magenta rectangles indicate shadows on the module rows (self-shading).

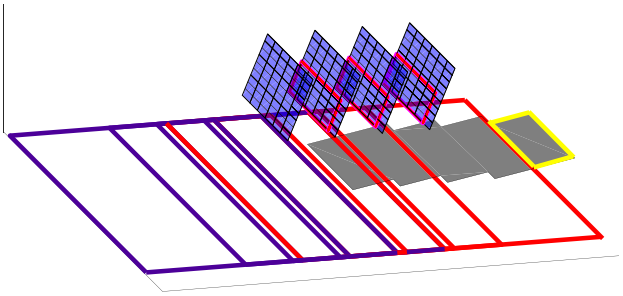

Fig. 5b. Interaction of cast ground shadows, which merged into a single shadow, with front (purple) and rear (red) view fields at time with self-shading. The yellow-contoured shadow area does not contribute to absorbed irradiation, since it is not part of any view field. The magenta rectangles indicate shadows on the module rows (self-shading).

irrespective of adjacent module rows. The main formulas used to calculate the energy yield are given in Section 6, Table 2.

2.5. Calculation of generated electricity

The model checks each cell string whether the front or rear is shaded or not, thereby emulating a bypass diode. If a string is shaded (fully or partially) by another module row, the corresponding bypass diode is forward biased, thus the power generation of the cell string is zero during the corresponding time step. The simulation was performed in a half-hourly resolution, where the hourly typical meteorological year (TMY) data was interpolated linearly. Losses due to inverters, wiring, soiling etc. were considered zero. For simplicity, the efficiency of maximum power point trackers was considered always as one.

2.6. Testing the model using a case study

The Chilean bifacial PV power plant La Hormiga in San Felipe (latitude = –32.7159°, longitude = −70.7221°) was taken as the reference for our case study (Fig. 6). La Hormiga incorporates 9,180 bifacial modules (270 W_p), as well as 240 monofacial modules[2] (ISC Konstanz, 2015). The technical parameters of the bifacial modules were taken from the "BiSoN MBA-GG60-270 W_p" datasheet (Megacell, 2015). According to photographs of the site (Joanny et al., 2017; Kopecek, 2018), the ground is covered with white gravel along the

[2] Because the focus of this work is on bifacial PV, the monofacial modules were neglected.

Fig. 6. Photograph of La Hormiga, taken in 2017 (Kopecek, 2018).

whole length of a module row in order to increase the energy yield. The ground surface to the left and right of a module row has not been modified. Since we had no possibility to measure the ground reflectivity onsite, a value of 40% was used for white gravel (Bretz et al., 1998). Furthermore, La Hormiga has three modules in landscape format along the short side of a row with a tilt angle of approximately 30°. The array's front is oriented towards the equator, the modules' installation height is roughly 0.5 m and the row spacing is approximately 5 m. This corresponds to a ground coverage ratio of 0.59, whereby this ratio is defined as the (usually) short side of a module row divided by the row spacing (Doubleday et al., 2016). A TMY dataset for San Felipe in hourly resolution was taken from (Ministerio de Energía, 2017). Since the simulation was carried out for both sides of each cell string, it would have been computationally too time-consuming to consider all modules of La Hormiga. Therefore, a downscaled PV power plant was simulated, which had four rows. Each row incorporated 18 modules in landscape format, with three modules along the short side and six along the bottom. In total, the investigated bifacial PV system had 72 bifacial modules with a front-side capacity of 19.44 kW_p.

3. Results & discussion

3.1. Absorbed irradiation & generated electricity

The energy yield was simulated over the course of one year. Fig. 7 shows the energy yield in terms of absorbed irradiation (subscript "ab"),

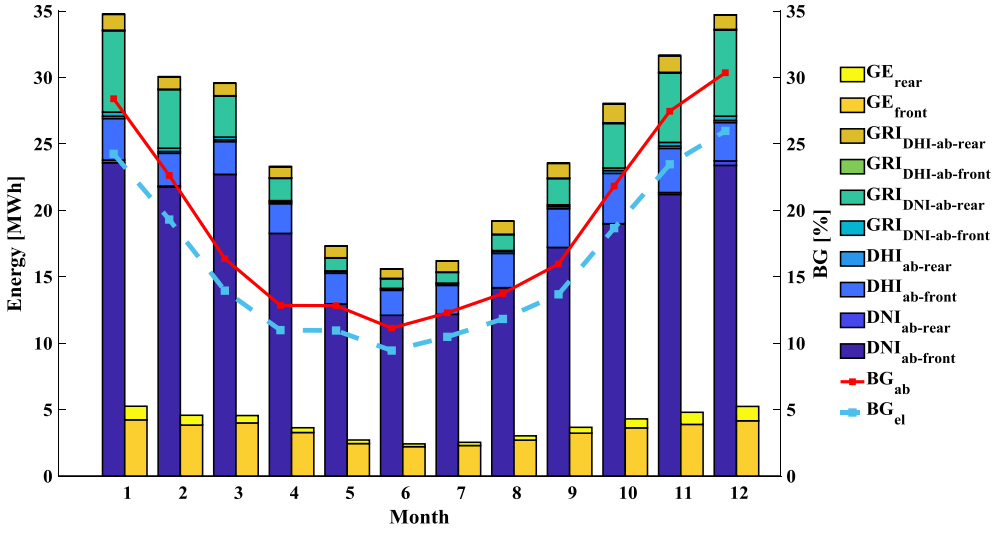

Fig. 7. Simulated absorbed irradiation, generated electricity (GE) and bifacial gains (BG_{ab}, BG_{el}) of a 19.44 kW_p bifacial PV power plant, located in San Felipe, Chile. Subscripts: "ab" = absorbed irradiation from corresponding irradiance contribution, "el" = electrical.

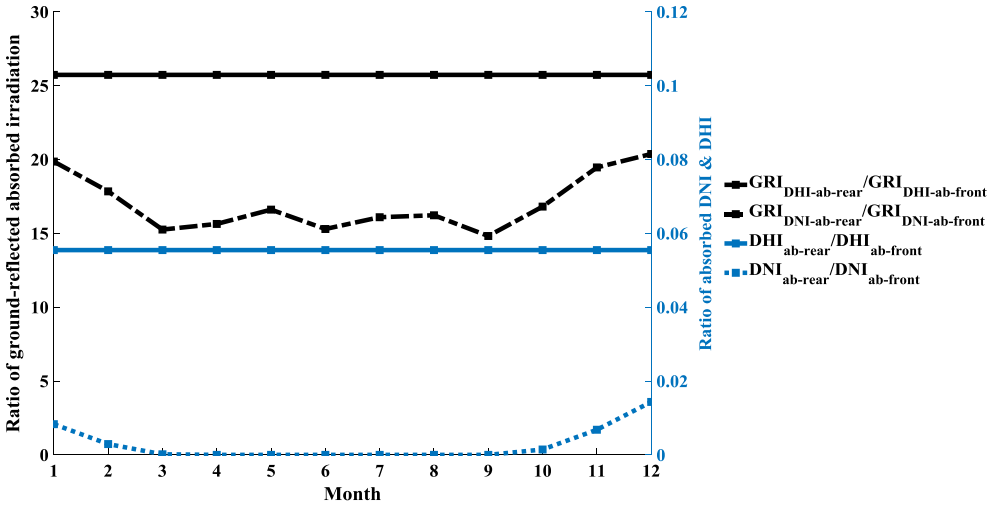

Fig. 8. Simulated monthly ratios of rear and front irradiation contributions.

generated electricity (GE) as well as bifacial gains. One can see that BG_{ab} and BG_{el} were higher in the summer months than in the wintertime.[3] This happens, because the sun's elevation angle is lower in winter and therefore reduces the intensity of GRI_{DNI}. Additionally, shadows are longer in winter and GRI_{DNI} is further reduced. The differences between BG_{ab} and BG_{el} arose, because both are coupled through the relationship: bifaciality $\varphi_{PV} = BG_{el}/BG_{ab}$ (when neglecting electrical losses). The major reason for the described divergence in both BG is that the bifaciality of the analysed modules is 0.85. Two electrical losses led to further decrease of the generated electricity. Firstly, the absorbed irradiation on the rear heated up the modules more, thus reducing the electrical efficiency. Secondly, partly shaded strings did absorb irradiation, but did not contribute to power generation due to the activated bypass diode. For the whole year, the loss in power generation due to self-shading was 0.2%. It should be noted, that this figure represents losses due to self-shading of the module rows only; shadows from mounting, junction boxes, nearby objects etc. were not considered in this work. Furthermore, Fig. 7 illustrates that in summer $GRI_{DNI\text{-}ab\text{-}rear}$ is significantly larger than $GRI_{DHI\text{-}ab\text{-}rear}$, while both contributions are roughly the same in winter months. This can be attributed to longer ground shadows in the winter as well, as well as to the use of an isotropic sky diffuse model. As expected, $DNI_{ab\text{-}front}$ constituted the greatest share of absorbed irradiation in every month, which is always true in sunny regions. The annual bifacial gains were BG_{ab} = 20.1% and BG_{el} = 17.1%. For optimized bifacial PV installations, a BG_{el} up to 30% can be expected (Kopecek and Libal, 2018). The "Bifacial Design Guide" from LG reports, that at a ground reflectivity of 90%, a BG_{el} of almost 29% is achievable (LG, 2017). For larger arrays with adverse interactions between module rows and ground shadows, lower values in the range of 5–15% can be expected, whereby these values strongly depend on the array design, location and especially the ground reflectivity (Reise and Schmidt, 2015). For the entire year, the specific electricity yields (SEY) were SEY_{front} = 2051 kWh_{dc}/kW_{front}, SEY_{rear} = 351 kWh_{dc}/kW_{front} and $SEY_{front+rear}$ = 2402 kWh_{dc}/kW_{front}.

3.2. Seasonality of rear and front irradiation contributions

Fig. 8 shows the monthly ratios of rear and front irradiation contributions. Both ratios from $GRI_{DHI\text{-}ab\text{-}rear/front}$ and $DHI_{ab\text{-}rear/front}$ were constant throughout the year, because they depended on the module slope angle only. The ratio of $DNI_{ab\text{-}rear/front}$ is characterized by a smooth course over the year, rising in summer and dropping in winter. This is due to the DNI only rarely hitting the rear and only for short periods during sunrise and sunset, which led to a minimal increase in $DNI_{ab\text{-}rear}$. The annual course of $GRI_{DNI\text{-}ab\text{-}rear/front}$ is characterized by a zigzag contour. This is based on two effects: firstly, when the sun is lower, the cast ground shadows are further away from the array, leading to fewer interactions between the ground shadows and the view fields. Secondly, when interaction takes place, the rear view fields are affected more often than the front view fields, because the array is oriented towards the equator and ground shadows were only rarely in front of the array (more precisely: when the beam irradiance hit the rear). One can also see that the rear contributes relatively more to $GRI_{DNI\text{-}ab\text{-}rear}$ in the summer months when the sun elevation angle is high. In summary, although $GRI_{DNI\text{-}ab\text{-}rear}$ and $GRI_{DHI\text{-}ab\text{-}rear}$ are significantly larger than $GRI_{DNI\text{-}ab\text{-}front}$ and $GRI_{DHI\text{-}ab\text{-}front}$ (provided that the modules are not installed vertically), the energy yield of the front might tip the scale when it comes to bankability considerations. It is therefore advisable to consider GRI_{front} in all yield predictions.

3.3. Influence of ground size on the energy yield

As previously mentioned, we defined front and rear view fields, which represent the ground contributing to GRI. The width of all view fields (VF) was initially defined as the 1.5-fold length of a module row by expanding its width by 25% to the left and the right of a module row. This corresponded to a VF width factor of 0.25 (a VF width factor of zero would mean that the width of all view fields is exactly the length of a module row). In order to investigate the impact of the view fields' width on the energy yield, a sensitivity analysis was conducted. Fig. 9 shows, that the enlargement of the VF width factor from zero to 0.25 gave the largest increase in energy yield. A further increase of the VF width factor promoted the energy yield insignificantly. This result reveals, that although the area of the view fields was increased proportionally, the course of the energy yield showed an asymptotical behaviour. This is because the longer the distance from a view field's segment to a module, the smaller the corresponding view factor. In conclusion, in order to boost the energy yield by increasing the ground reflectivity (e.g., using bright ground cover material), it might be enough to consider the ground in close vicinity only, thereby saving costs.

3.4. Influence of ground shadows on the energy yield

Based on the previously mentioned assumptions regarding completely opaque modules, cast ground shadows do not reflect DNI, thus reducing the energy yield of the power plant. In order to assess the magnitude of this effect, a second scenario was simulated. In this

[3] In the southern hemisphere, the seasons are the other way around than in the northern hemisphere.

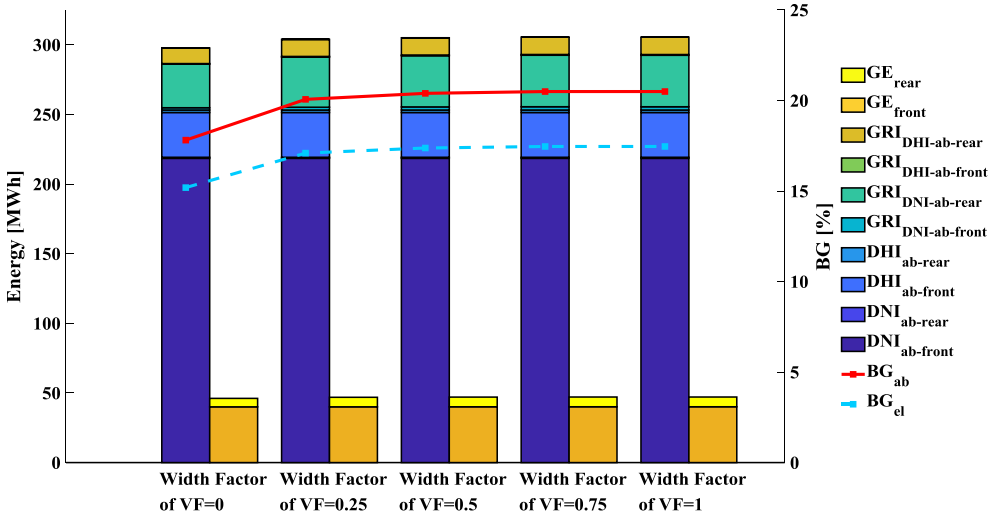

Fig. 9. Impact of the view fields' width on the annual energy yield and bifacial gains.

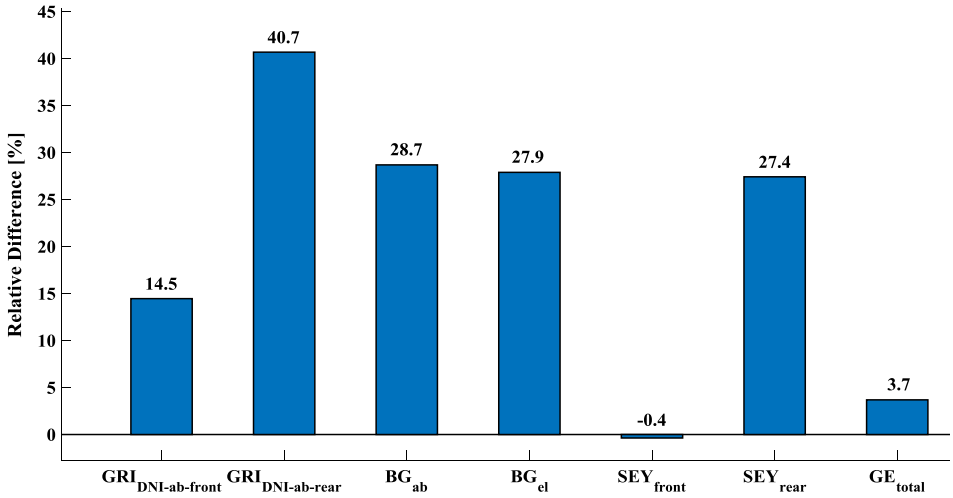

Fig. 10. Relative difference of selected parameters based on two scenarios: 1. Cast ground shadows do not exist; 2. Cast ground shadows exist.

Table 1
Different ground surfaces and their reflectivity.

Ground surface	Ground reflectivity [%]	Reference
Dry Asphalt	12	PVsyst (n.d.)
Grass	20	PVsyst (n.d.)
Dry Grassland	25	Intelligent Systems Laboratory (n.d.)
White Gravel	40	Bretz et al. (1998)
White Membrane	70	Bretz et al. (1998)

second scenario, all boundary conditions were unchanged except one: there were no ground shadows, (i.e., all view fields were always unshaded). However, self-shading among the module rows still occurred. Through the comparison of this second scenario with the primary one, we derived the influence of the ground shadows on the power plant's performance. Fig. 10 shows the relative difference[4] of selected parameters related to a whole year. It reveals that cast ground shadows affected $GRI_{DNI\text{-}ab\text{-}rear}$ the most, reducing its contribution by more than 40%. Interestingly, SEY_{front} was slightly lower when there were no ground shadows. This happened, because the effect of additional heating of the modules, which reduced the electrical efficiency, outweighed the amount of additional $GRI_{DNI\text{-}ab\text{-}front}$. SEY_{rear} would have been 27% higher if there were no ground shadows. In addition, the total annual electricity generation GE_{total} would have grown by 3.7%. It is worth mentioning that all values highly depend on the view fields' size and ground reflectivity. Nevertheless, the magnitude of results show that cast shadows can have a significant impact on a bifacial PV power plant's performance and their adequate modelling is advisable.

3.5. Increasing the energy yield with bright ground covering

The ground reflectivity is one of the most important parameters for the energy yield of a bifacial PV power plant. The power plant's operator can artificially adjust this parameter for maximizing the energy yield. In order to quantify the change in energy yield when using different ground surfaces, a sensitivity analysis with five different ground surfaces (Table 1) was performed. The resulting annual energy yield and bifacial gains are presented in Fig. 11. The comparison of different ground surfaces illustrates that the use of bright ground cover materials (white gravel, white membrane) significantly increases the annual electricity yield.

[4] Relative Difference = ($Parameter_{no\ ground\ shadows}$ - $Parameter_{with\ ground\ shadows}$)/$Parameter_{with\ ground\ shadows}$.

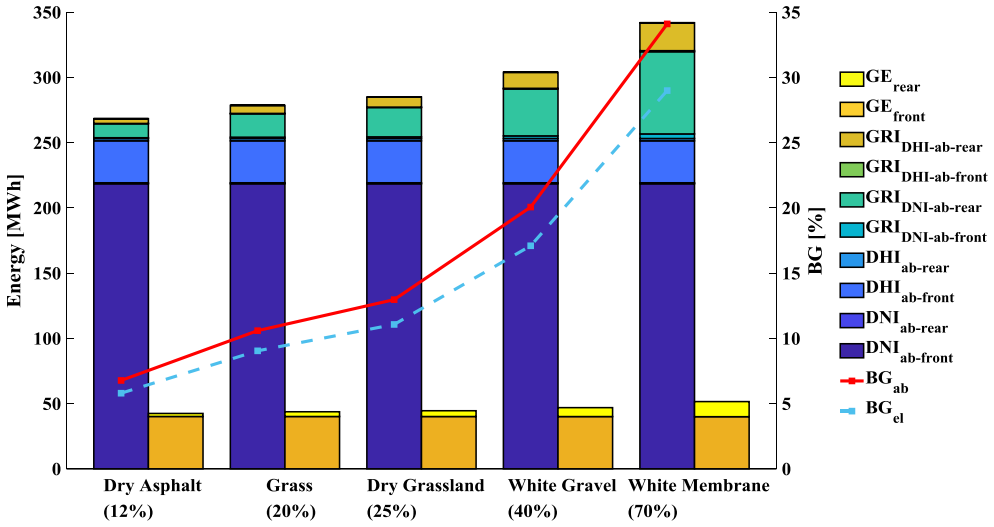

Fig. 11. Sensitivity analysis of ground reflectivity.

4. Conclusion & outlook

Based on a review of existing models to simulate the energy yield of bifacial PV power plants, this work explores options to improve the quality of energy yield models. The presented opportunities for improvement were implemented in an own simulation model, where the influence of ground size, cast ground shadows as well as ground reflectivity on the energy yield were investigated. The breakdown of absorbed irradiation originating from eight irradiance contributions ($DNI_{front/rear}$, $DHI_{front/rear}$, $GRI_{DHI\text{-}front/rear}$ and $GRI_{DNI\text{-}front/rear}$, whereby GRI stands for ground-reflected irradiance) allowed for the identification of the most significant contributions to the total energy yield. The presented method shows how the influence of ground shadows on the entire PV array can be accounted for in a holistic way. This means that it should be accounted for that the cast ground shadows of any module row may have an impact on absorbed GRI by any other row.

A 19.44 kW_p bifacial PV power plant, based on technical characteristics of the Chilean bifacial PV power plant La Hormiga was used as a case study to test the model. The results showed that the monthly bifacial gain regarding absorbed irradiation (BG_{ab}) was on average two percentage points higher than the bifacial gain regarding generated electricity (BG_{el}). Annual BG_{el} and BG_{ab} were 17.1% and 20.1%, respectively, where the ground surface was white gravel with a reflectivity of 40%.

To evaluate the impact of the ground size on the energy yield, a sensitivity analysis was conducted. The results showed that the extension of ground area, which contributes to ground-reflected irradiation, resulted in a slight, asymptotical increase of the energy yield.

In order to investigate the impact of ground shadows on the power plant's performance, a scenario without ground shadows was simulated. It was possible to show that $GRI_{DNI\text{-}ab\text{-}rear}$ was reduced more than any other irradiation contribution and would have been around 40% higher if there were no ground shadows. Annual electricity generation would have risen by nearly 4%.

Finally, the influence of ground reflectivity on the energy yield was investigated. Using five different ground surfaces (dry asphalt, grass, dry grassland, white gravel and white membrane), the change in annual energy yield and bifacial gains was analysed. It became apparent, that the use of bright ground cover materials significantly increased the annual energy yield: in the case of white membrane (70% reflectivity), BG_{el} grew to 29%.

Future improvements of the presented simulation model can be achieved by allowing spatial (e.g., partially covering the ground with bright gravel) and temporal (season-dependent) variations of the ground reflectivity. Furthermore, it should be taken into account that bifacial modules are semi-opaque. Finally, provided that necessary datasets will become available, the model should be validated against real field measurements.

Acknowledgement

The authors are grateful for the support of the German Federal Ministry of Education and Research through Grant number 01DN15008 and the support of the Chilean Council of Scientific and Technological Research through the Solar Energy Research Center SERC-Chile (CONICYT/FONDAP/15110019) and the Solar Mining project (Program for International Cooperation/CONICYT-BMBF/20140019). Simón Moreno-Leiva would like to thank the support of the German Academic Exchange Service (DAAD) and the National Commission for Scientific and Technological Research of Chile (CONICYT) through the "Becas Chile-DAAD" program.

Appendix

Table 2 shows the main formulas to calculate the energy yield for the case that beam irradiance comes from the front. For the case of beam light hitting the rear, the same formulas apply (with necessary changes in the subscripts).

Table 2
Formulas for the calculation of absorbed irradiation and generated electricity.

Direct light incidence on the front, cell string is unshaded			
$DNI_{ab\text{-}front}$ & $DHI_{ab\text{-}front}$	$GRI_{ab\text{-}front}$	$GRI_{ab\text{-}rear}$	Generated Electricity
$E_{abCell\ String,front} = [DNI{\cdot}\cos(\Theta) + DHI{\cdot}V_{Cell\ String\rightarrow Sky}]$ $\cdot A_{String,unshaded}{\cdot}\alpha_{PV}$	$E_{abCell\ String,front,\ GRI}=[DHI{\cdot}A_{RVF_{complete}}{\cdot}V_{FVF_{complete}\rightarrow Cell\ String}$ $+\ DNI{\cdot}\cos(\theta_z){\cdot}A_{RVF_{Reduced}}{\cdot}V_{FVF_{Reduced}\rightarrow Cell\ String}]{\cdot}GR{\cdot}\alpha_{PV}$	$E_{abCell\ String,rear,\ GRI}=[DHI{\cdot}A_{RVF_{complete}}{\cdot}V_{RVF_{complete}\rightarrow Cell\ String}$ $+\ DNI{\cdot}\cos(\theta_z){\cdot}A_{RVF_{Reduced}}{\cdot}V_{RVF_{Reduced}\rightarrow Cell\ String}]{\cdot}GR{\cdot}\alpha_{PV}$	$E_{abCell\ String} = \eta_{PV,front}{\cdot}[E_{abCell\ String,front}$ $+E_{abCell\ String,front,\ GRI}$ $+E_{abCell\ String,rear,\ GRI}{\cdot}\phi_{PV}]$
Direct light incidence on the front, cell string is shaded			
$DNI_{ab\text{-}front}$ & $DHI_{ab\text{-}front}$	$GRI_{ab\text{-}front}$	$GRI_{ab\text{-}rear}$	Generated Electricity
$E_{abCell\ String,front} = [DNI{\cdot}\cos(\theta) + DHI{\cdot}V_{Cell\ String\rightarrow Sky}]$ $\cdot A_{Cell\ String,shaded}{\cdot}\alpha_{PV}$	see above	see above	0
Calculation of $\eta_{PV,\ front}$			
$\eta_{PV,front} = \eta_{PV,front,ref}{\cdot}[1 - \beta{\cdot}(T_{amb} - T_{ref}) + (T_{NOCT} - T_{amb}){\cdot}\frac{I_{sum}}{I_{NOCT}}]$ Dubey et al. (2013)			

References

Appelbaum, J., 2016. Bifacial photovoltaic panels field. Renew. Energy 85, 338–343.

Berrian, D., Libal, J., Glunz, S., 2017. MoBiDiG: Simulat. LCOE.

Bretz, S., Akbari, H., Rosenfeld, A., 1998. Practical issues for using solar-reflective materials to mitigate urban heat islands. Atmos. Environ. 32 (1), 95–101.

Chiodetti, M., Guédez, R., Lindsay, A., 2015. Bifacial PV Plants: Performance Model Development and Optimization of Their Configuration. KTH Royal Institute of Technology. http://kth.diva-portal.org/smash/get/diva2:848584/FULLTEXT01.pdf. Accessed 15 February 2017.

DiOrio, N., Deline, C., 2018. Bifacial simulation in SAM. Bifacial Workshop 2018. <http://bifipv-workshop.com/fileadmin/images/bifi/denver/presentations/4_Diorio-_Modeling_with_SAM_bifiPV2018.pdf> (Accessed 9 October 2018).

Doubleday, K., Choi, B., Maksimovic, D., Deline, C., Olalla, C., 2016. Recovery of inter-row shading losses using differential power-processing submodule DC–DC converters. Sol. Energy 135, 512–517.

Dubey, S., Sarvaiya, J.N., Seshadri, B., 2013. Temperature dependent photovoltaic (PV) efficiency and its effect on PV production in the world – a review. Energy Proc. 33, 311–321.

Duffie, J.A., Beckman, W.A., 2013. Solar Engineering of Thermal Processes, fourth ed.

Gross, U., Spindler, K., Hahne, E., 1981. Shapefactor-equations for radiation heat transfer between plane rectangular surfaces of arbitrary position and size with parallel boundaries. Lett. Heat Mass Transf. 8 (3), 219–227.

Intelligent Systems Laboratory, n.d. Average Ground Reflectance Info. <http://www.intelligence.tuc.gr/renes/fixed/info/reflectanceinfo.html> (Accessed 8 October 2018).

Konstanz, I.S.C., 2015. Largest bifacial PV system by MegaCell with BiSoN modules in Hormiga, Chile. Accessed 6 April 2018. http://isc-konstanz.de/isc/aktuelles/news/article/larges-bifacial-pv-system-build-by-megacell-with-bison-modules-in-hormiga-chile.html.

Ishikawa, N., 2016. World First Large Scale 1.25MW Bifacial PV Power Plant on Snowy Area in Japan. 3rd bifi PV workshop in Miyazaki, Japan. Photovoltaic Technical Solutions. <http://bifipv-workshop.com/fileadmin/images/bifi/miyazaki/presentations/3_1_3_-_ISHIKAWA_-_World_1st_large_scale_Bifacial_PV_power_plant.pdf> (Accessed 15 February 2017).

Janssen, G.J.M., Burgers, A.R., Binani, A., Carr, A.J., van Aken, B.B., Romjin, I., Klenk, M., Nussbaumer, H., Baumann, T., 2018. How to maximize the kWh/kWp ratio: simulations of single-axis tracking in bifacial systems.

Joanny, M., Libal, J., Kopecek, R., Veschetti, Y., Colin, H., 2017. Bifacial Systems Overview. <http://bifipv-workshop.com/fileadmin/layout/images/Konstanz-2017/1_M._Joanny_INES_System_overview.pdf> (Accessed 7 February 2018).

Khan, M.R., Hanna, A., Sun, X., Alam, M.A., 2017. Vertical Bifacial Solar Farms. Physics, Design, and Global Optimization. <http://arxiv.org/pdf/1704.08630>.

Kopecek, R., 2014. Bifacial world – monofacial modules: why do we compromise system power? <http://de.slideshare.net/sandiaecis/2-kopecek-bifi-pvok-60345232> (Accessed 15 February 2017).

Kopecek, R., 2018. Photos from bifacial PV power plant “La Hormiga”. Personal Communication.

Kopecek, R., Libal, J., 2018. Towards large-scale deployment of bifacial photovoltaics. Nat. Energy 3 (6), 443–446.

Lauzier, N., 2004. MATLAB function that calculates view factors between two planar surfaces. <https://de.mathworks.com/matlabcentral/fileexchange/5664-view-factors> (Accessed 14 July 2017).

LG, 2017. Bifacial Design Guide. <http://www.lg-solar.com/downloads/brochures/Bifacial_design_guide_Full_ver.pdf> (Accessed 25 January 2018).

Maor, T., Appelbaum, J., 2012. View factors of photovoltaic collector systems. Sol. Energy 86 (6), 1701–1708.

Marion, B., MacAlpine, S., Deline, C., 2017. A Practical Irradiance Model for Bifacial PV Modules. Preprint. <https://www.nrel.gov/docs/fy17osti/67847.pdf> (Accessed 9 October 2018).

Megacell, 2015. Datasheet BiSoN MBA-GG60 series 270-280Wp. <http://www.mega-group.it/wp-content/uploads/MBA-GG60-270_280B_rev3.pdf> (Accessed 5 April 2018).

Mermoud, A., Wittmer, B., 2017. Bifacial shed simulations with PVsyst. <http://bifipv-workshop.com/fileadmin/layout/images/Konstanz-2017/2_B._Wittmer_PV_SYST_Bifacial_shed_simulations.pdf>.

Meydbray, J., 2018. Barriers to Financing Bifacial PV Projects. <http://bifipv-workshop.com/fileadmin/images/bifi/denver/presentations/1_Meydbrey-_financing_barriers_bifiPV2018.pdf> (Accessed 18 October 2018).

Ministerio de Energía, 2017. Explorador Solar. <http://www.minenergia.cl/exploradorsolar/> (Accessed 14 September 2017).

PVsyst, n.d. Albedo coefficient. <http://files.pvsyst.com/help/albedo.htm>. Accessed 8 October 2018.

Reise, C., Schmidt, A., 2015. Realistic Yield Expectations for Bifacial PV Systems – an Assessment of Announced, Predicted and Observed Benefits. Frauenhofer ISE. <https://www.tuv.com/media/corporate/solar_1/pv_modulworkshop_2/42_Reise_

Realistic_Yield_Expectations_for_Bifacial_PV_Systems.pdf> (Accessed 4 May 2018).
Richter, A., 2017. Bankability. Meyer Burger. <http://bifipv-workshop.com/fileadmin/layout/images/Konstanz-2017/1_A._Richter_MEYER_BURGER_Bankability.pdf> (Accessed 18 October 2018).
Shoukry, I., Libal, J., Kopecek, R., Wefringhaus, E., Werner, J., 2016. Modelling of bifacial gain for stand-alone and in-field installed bifacial PV modules. Energy Proc. 92, 600–608.
Stephan, P., Kabelac, S., Kind, M., Martin, H., Mewes, D., Schaber, K.-H., 2010. VDI Heat Atlas, 2. Springer, Heidelberg u.a XXI, 1585 S.
VDMA, 2017. International Technology Roadmap for Photovoltaic (ITRPV). 2016 Results. <http://www.itrpv.net/Reports/Downloads/> (Accessed 2 July 2017).
Yusufoglu, U.A., Lee, T.H., Pletzer, T.M., Halm, A., Koduvelikulathu, L.J., Comparotto, C., Kopecek, R., Kurz, H., 2014. Simulation of energy production by bifacial modules with revision of ground reflection. Energy Proc. 55, 389–395.